

# A Study of how LaFeO<sub>3</sub> and CaTiO<sub>3</sub> Supports Affect the Oxidation, Hydrogenation, and Methane Steam Reforming Activity of Pt and Ni Catalysts

Siwon Lee<sup>1</sup>, Matteo Monai<sup>2</sup>, Kai Shen<sup>1</sup>, Jian Chang<sup>1</sup>, John M. Vohs<sup>1,\*</sup>, Raymond J. Gorte<sup>1</sup>

<sup>1</sup>Department of Chemical and Biomolecular Engineering, University of Pennsylvania, Philadelphia, Pennsylvania 19104, United States

<sup>2</sup>Inorganic Chemistry and Catalysis Group, Debye Institute for Nanomaterials Science, Utrecht University, Universiteitsweg 99, 3584 CG Utrecht, The Netherlands

**Keywords:** Platinum, Nickel, Perovskites, Catalysts, Oxidation, Hydrogenation, Methane steam reforming, Atomic layer deposition, Redox reactions

**Corresponding author:** John M. Vohs (vohs@seas.upenn.edu)

## Abstract

The structure and catalytic properties of Pt and Ni supported on thin films of LaFeO<sub>3</sub> and CaTiO<sub>3</sub>, prepared by Atomic Layer Deposition (ALD), were investigated. X-Ray diffraction (XRD) and scanning transmission electron microscopy (STEM) show that reduction at 1073 K causes Pt-Fe intermetallic compound formation for Pt/LaFeO<sub>3</sub>. For Pt/CaTiO<sub>3</sub>, 1073-K reduction induces local decomposition of the CaTiO<sub>3</sub> with migration of Ti to the Pt. Reduced Pt/LaFeO<sub>3</sub> and Pt/CaTiO<sub>3</sub> exhibited CO-oxidation activity similar to that for Pt supported on MgAl<sub>2</sub>O<sub>4</sub> but were much less active for propane oxidation and hydrogenation of 1-hexene and toluene. In contrast, Ni/CaTiO<sub>3</sub> behaved similarly to a conventional supported Ni catalyst for the methane-steam-reforming (MSR) and 1-hexene hydrogenation. There was also no evidence for local decomposition of the perovskite in the vicinity of the Ni particles. The results obtained in this study demonstrate that metal-perovskite interactions that affect reactivity are specific to each component.

## Introduction

There has been significant interest in perovskites as supports for metal catalysts because of their ability to maintain high metal dispersion in high-temperature applications. This is due, at least in some cases, to the fact that large metal particles can be redispersed by reversible ingress and egress of metal cations from the perovskite lattice<sup>1, 2, 3, 4, 5</sup>. This latter process is often referred to as exsolution<sup>6, 7</sup>. Although this aspect of perovskite-supported metals is intriguing, there have been few practical applications of these systems. Major problems include that: (1) most perovskites have low surface areas, (2) the kinetics of metal exsolution are too slow at reasonable temperatures<sup>8</sup>, and (3) some of the exsolved metal can remain embedded in the bulk and unavailable for reaction<sup>9</sup>. Our groups have been working on a potential solution to these problems by preparing thin films of various mixed perovskites on inert supports using Atomic Layer Deposition (ALD)<sup>10, 11, 12, 13</sup>. We have shown that using this approach one can produce two-dimensional, perovskite crystallites with lateral dimensions as large as 20 nm and thicknesses as thin as 0.5 nm<sup>13, 14</sup>. Because a 0.5-nm film of LaFeO<sub>3</sub> on 120-m<sup>2</sup>/g support corresponds to nearly 28-wt% LaFeO<sub>3</sub><sup>15, 16</sup>, such films will have sufficient capacity for taking up metal cations; but, in contrast to bulk perovskite supports, the catalytic metals will remain at or near the surface.

While the main goal in using perovskites as supports was for maintaining metal dispersion, catalytic studies have shown that these materials have other interesting characteristics. One of the first reports of novel catalytic properties was the demonstration that Ni exsolving from bulk La<sub>0.4</sub>Sr<sub>0.4</sub>Ni<sub>0.03</sub>Ti<sub>0.97</sub>O<sub>3-δ</sub>, exhibited greatly increased tolerance against coking in the presence of dry CH<sub>4</sub> at high temperatures<sup>17</sup>. This result was later duplicated with Ni on CaTiO<sub>3</sub> films<sup>18</sup> in a study that showed that the CaTiO<sub>3</sub>-supported Ni retained high activity for CH<sub>4</sub> reforming after many oxidation-reduction cycles at 1073 K. Another example is Pt supported on CaTiO<sub>3</sub> films, a catalyst that exhibited similar activity for CO oxidation to a conventional supported Pt catalyst but was much less active for toluene hydrogenation<sup>19</sup>. Interestingly, metal-support interactions with CaTiO<sub>3</sub> were shown to be metal-specific, since, unlike Pt, the dispersion and catalytic properties of Pd were not affected by a CaTiO<sub>3</sub> support<sup>5, 19</sup>.

We do not yet have a good understanding of why perovskite-supported metals are catalytically different. It has been suggested that the carbon tolerance observed with Ni exsolving from La<sub>0.4</sub>Sr<sub>0.4</sub>Ni<sub>0.03</sub>Ti<sub>0.97</sub>O<sub>3-δ</sub> originates from the fact that the exsolved metal particles remain partially embedded in the support<sup>20</sup>, but this is unlikely to explain the carbon tolerance observed

with Ni on 1.0-nm films of CaTiO<sub>3</sub><sup>18</sup>. Changes in the shapes of Pt particles on CaTiO<sub>3</sub><sup>19</sup> and their orientation on LaFeO<sub>3</sub><sup>11</sup> suggest local bonding interactions with the support are important. This conclusion is supported by the aforementioned observation that metal-perovskite interactions are metal specific (e.g., CaTiO<sub>3</sub> influences Pd and Pt differently<sup>19</sup>). Finally, thermodynamic measurements of Ni-NiO equilibria for Ni catalysts supported on LaFeO<sub>3</sub><sup>21</sup> and ATiO<sub>3</sub> (A=Ca, Sr, and Ba)<sup>22</sup> showed changes consistent with the perovskites affecting the chemical state of the Ni.

In the present work, we investigated the nature of perovskite-metal interactions for Ni and Pt catalysts on CaTiO<sub>3</sub> and LaFeO<sub>3</sub> thin films by comparing reaction rates for these catalysts to those for Pt/MgAl<sub>2</sub>O<sub>4</sub> and Ni/MgAl<sub>2</sub>O<sub>4</sub> for a range of reactions, including CO and propane oxidations, 1-hexene and toluene hydrogenations, and methane-steam reforming (MSR). Consistent with previous reports, the perovskite supports were found to be effective in maintaining metal dispersion even after redox cycling at 1073 K. With the exception of CO oxidation, the rates of reactions on both CaTiO<sub>3</sub>- and LaFeO<sub>3</sub>-supported Pt were much lower than those on conventional Pt catalysts. X-ray diffraction (XRD) data suggest that this is due to Pt-Ti and Pt-Fe alloy formation on the reduced catalysts. While high-temperature reduction was necessary to activate Ni/CaTiO<sub>3</sub>, the reduced catalysts showed similar activities as a conventional Ni catalyst for the reactions studied.

## Experimental

The catalysts that were examined in this study are listed in **Table 1**, with most prepared by Atomic Layer Deposition (ALD) of the catalytic components onto either MgAl<sub>2</sub>O<sub>4</sub> or La-doped Al<sub>2</sub>O<sub>3</sub> (4-wt% La<sub>2</sub>O<sub>3</sub>, referred to here as La-Al<sub>2</sub>O<sub>3</sub>) supports. The MgAl<sub>2</sub>O<sub>4</sub> support was prepared by co-precipitation of Mg and Al salts as described previously<sup>18</sup>. After calcination to 1173 K for 12 h, its BET surface area was 120 m<sup>2</sup>/g. The La-Al<sub>2</sub>O<sub>3</sub> was provided to us by Johnson-Matthey and had a surface area of 195 m<sup>2</sup>/g. ALD was performed using equipment and procedures that are described only briefly here but, in more detail, elsewhere<sup>11, 18, 19, 23</sup>. The ALD procedure consisted of exposing evacuated supports to a few Torr of the precursor of interest for 10 min at temperatures between 473 K to 523 K, depending on the precursor. Following evacuation of the excess precursor, the samples were removed from the high-temperature adsorption apparatus and calcined in a muffle furnace at either 773 K (for Pt) or 873 K (for the other precursors) to remove the ligands

from the adsorbed precursor. The exception to this was TiO<sub>2</sub>, since the Cl<sup>-</sup> anions could be removed by exposure to water vapor without transfer to the muffle furnace. The samples were then placed back in the adsorption apparatus and the cycle was repeated. For the perovskite films, the precursor exposures were alternated in the ratios required to give the correct oxide stoichiometries<sup>11,18</sup>.

**Table 1.** Properties of the samples used in this study

Sample	Metal loading (wt %)	Metal oxide loading (wt %)	BET surface area (m <sup>2</sup> /g)	Final pretreatment conditions	Dispersion	
					Measured <sup>a</sup>	Estimated <sup>b</sup>
Pt/MgAl <sub>2</sub> O <sub>4</sub>	4.9	-	96	773 K oxidation	31	27
				1073 K oxidation	2	6
Pt/LaFeO <sub>3</sub> / La-Al <sub>2</sub> O <sub>3</sub>	3.0	30	70	1073 K oxidation	0	5
				1073 K reduction	0	100
Pt/LaFeO <sub>3</sub> / MgAl <sub>2</sub> O <sub>4</sub>	3.1	28	78	1073 K reduction	-	-
Pt/Bulk LaFeO <sub>3</sub>	-	-	5	1073 K oxidation	0	-
				1073 K reduction	0	-
Pt/FeO <sub>x</sub> / MgAl <sub>2</sub> O <sub>4</sub>	3.2	14	77	1073 K oxidation	0	157
				1073 K reduction	3	117
Ni/MgAl <sub>2</sub> O <sub>4</sub>	3.7	-	96	773 K reduction	-	-
				1073 K reduction	-	-
Ni/CaTiO <sub>3</sub> / MgAl <sub>2</sub> O <sub>4</sub>	4.4	29	74	773 K reduction	-	-
				1073 K reduction	-	-
Pt/CaTiO <sub>3</sub> / MgAl <sub>2</sub> O <sub>4</sub>	2.9	30	84	1073 K oxidation	0	-
				1073 K reduction	0	-

<sup>a</sup> Dispersions measured by CO chemisorption experiments

<sup>b</sup> Dispersions estimated from the specific reaction rate of CO oxidation reported in the literature<sup>26</sup>

The precursors used for ALD were La(TMHD)<sub>3</sub> (TMHD = tris(2,2,6,6-tetramethyl-3,5-heptanedionato), Strem Chemicals, Inc.), ferrocene (Fe(Cp)<sub>2</sub>, Sigma-Aldrich), Ca(TMHD)<sub>2</sub> (Strem

Chemicals, Inc.),  $\text{TiCl}_4$  (Sigma-Aldrich, USA),  $\text{Pt}(\text{acac})_2$ , (platinum (II) acetylacetonate, Sigma Aldrich), and  $\text{Ni}(\text{TMHD})_2$  (Strem Chemicals, Inc.). Growth rates, in atoms per gram of support, were determined gravimetrically and corroborated using ICP-OES. Film thicknesses were calculated from the mass increases and BET surface areas, assuming a bulk density for the films. In all cases, the film growth rates were linear, ranging from 0.015 nm/cycle (for CaO) to 0.030 nm/cycle (for  $\text{Fe}_2\text{O}_3$ ).

To demonstrate that the catalytic properties of Pt on thin-film  $\text{LaFeO}_3$  were similar to that of Pt on bulk  $\text{LaFeO}_3$ , a bulk  $\text{LaFeO}_3$  sample was prepared using nitrate salts of the two metal-oxide components,  $\text{La}(\text{NO}_3)_3 \cdot 6\text{H}_2\text{O}$  (Sigma Aldrich) and  $\text{Fe}(\text{NO}_3)_3 \cdot 9\text{H}_2\text{O}$  (Sigma Aldrich). The salts were dissolved in distilled water together with citric acid in a 1:1 ratio with the metal ions, then heated until the mixture became a viscous gel. The dried gel was ground to form a powder and calcined at 1173 K for 6 h. Pt was added by 1 ALD cycle. Although direct comparison of rates on the bulk and thin-film supports was not possible due to the large difference in surface areas, the relative rates of different reactions could be compared.

Because metal particle size can affect reaction rates for structure-sensitive reactions, the Pt/ $\text{MgAl}_2\text{O}_4$  catalyst was calcined at either 773 K or 1073 K in order to vary the metal dispersion. Because high-temperature oxidation is required to induce metal-perovskite interactions<sup>19</sup>, the other Pt catalysts (i.e., Pt/ $\text{LaFeO}_3$ / $\text{La-Al}_2\text{O}_3$ , Pt/ $\text{CaTiO}_3$ / $\text{MgAl}_2\text{O}_4$ , and Pt/ $\text{FeO}_x$ / $\text{MgAl}_2\text{O}_4$ ) were subjected to at least one redox cycle, consisting of oxidation at 1073 K, followed by reduction at 1073 K. As reported in previous studies, the perovskite-supported catalysts did not change with subsequent oxidation or reduction treatments at 1073 K but were strongly affected by whether the last step was an oxidation or reduction<sup>11, 19</sup>. All of the Ni catalysts were oxidized at 1073 K, then reduced at either 773 K or 1073 K.

Scanning Transmission Electron Microscopy (STEM) images with Energy Dispersive X-ray Spectra (EDS) were acquired on a JEOL JEM-F200 operated at 200 kV. The crystal structures were characterized by X-ray diffraction (XRD) using a RIGAKU SmartLab diffractometer (Cu  $K\alpha$  radiation). The Brunauer–Emmett–Teller (BET) and CO chemisorption experiments were carried out using home-built equipment. For CO chemisorption, each sample (100 mg) was first oxidized at 773 K for 10 min in a muffle furnace to remove residual organic matter, then transferred to the adsorption apparatus. The sample was then heated to 473 K in 300 Torr  $\text{H}_2$  for 10 min, followed by evacuation. The reduction-evacuation process was repeated three times before cooling

to 298 K for CO adsorption measurements. Dispersions were calculated assuming adsorption of one CO molecule per surface Pt. Extents of reduction of the selected samples were obtained by Flow Titration (FT)<sup>21</sup>. In each FT experiment, 100-mg samples were first reduced in a tubular reactor at 1073 K. After purging with dry He, oxygen uptakes were measured by flowing dry air (5 mL/min) over the sample while monitoring the effluent concentration using mass spectrometer. The amount of oxygen required to re-oxidize the sample was calculated by integrating the difference between N<sub>2</sub> and O<sub>2</sub> signals.

Rate measurements for CO oxidation, propane oxidation, and MSR were performed using a tubular flow reactor with an on-line gas chromatograph (GC, SRI Instruments Model 8610C, HayeSep Q column and Thermal Conductivity Detector (TCD)). In a typical experiment, a 100-mg sample was placed in the center of a quartz tube that had an inner diameter of a 6.35 mm. Quartz-wool plugs were inserted at each end to keep the catalyst in place. For CO oxidation, the feed was 28 Torr CO and 14 Torr O<sub>2</sub> in He, with a total flow rate of 100 mL min<sup>-1</sup>. Propane oxidation was carried out with 15 Torr of C<sub>3</sub>H<sub>8</sub> and 152 Torr of O<sub>2</sub> in He and a total flow rate of 110 mL min<sup>-1</sup>. Rates for MSR were measured using 38 Torr CH<sub>4</sub> and 76 Torr H<sub>2</sub>O at a flow rate of 110 mL min<sup>-1</sup>. Conversions were kept below 10% in order to maintain differential conditions. The hydrogenation of 1-hexene (97%, Acros Organics) and toluene (99.9%, Sigma Aldrich) were conducted in a separate, stainless-steel, tubular reactor with a 4.6-mm inner diameter. The online detector for this reactor was a GC/mass spectrometer (GC-MS, Shimadzu Model QP-5000). For 1-hexene hydrogenation, either 50 mg of a Pt-based catalyst or 100 mg of a Ni-based catalyst was loaded into the center of the tube. For toluene hydrogenation, the catalyst loading was always 100 mg. The liquid feeds were introduced to the reactor using a syringe pump (KDS 100 from KD Scientific) at a rate of 0.2 mL h<sup>-1</sup> and the gas feed was controlled using a mass flow controller (MFC, L-3441G from Omega Engineering). For 1-hexene hydrogenation, the gas feed was 3 mL min<sup>-1</sup> H<sub>2</sub> and 55 mL min<sup>-1</sup> He; for toluene hydrogenation, the gas feed was 70 mL min<sup>-1</sup> of H<sub>2</sub>. Rates were measured as a function of temperature and reported on Arrhenius plots. Activation energies for each of the reactions are reported in **Table S1**.

*Operando* Diffuse Reflectance Infrared Fourier Transform Spectroscopy (DRIFTS) was carried out using a Harrick high-temperature DRIFTS cell, situated in a Bruker Tensor 37 FTIR spectrometer equipped with a mercury cadmium telluride (MCT) detector. The catalyst powders were sieved to the 150–75 μm fraction and reduced or oxidized *ex situ* in a tubular oven at 1073 K

for 1 h under 1 bar 50 % H<sub>2</sub>/N<sub>2</sub> or 20 % O<sub>2</sub>/N<sub>2</sub>, respectively. After pre-treatment, 10 mg of powder were loaded in the DRIFTS cell and tested for CO oxidation under a total gas flow rate of 50 mL/min, using a N<sub>2</sub> carrier and partial pressures of CO and O<sub>2</sub> of 50 and 25 Torr, respectively. The reaction gases were introduced at 298 K for 10 min, after which the temperature was ramped at 5 K /min to 423 K and then to 513 K, with spectra measured for 30 min at each temperature. Finally, the cell was cooled to 298 K under reaction conditions to check for CO adsorption at lower temperatures. All gases were introduced through Bronkhorst EL-FLOW MFCs. During the experiments, DRIFTS spectra were collected with a time resolution of 1 spectrum/minute.

## Results

### *XRD and STEM*

#### *Pt-LaFeO<sub>3</sub>*

Previous studies of ALD-deposited LaFeO<sub>3</sub> films were performed on MgAl<sub>2</sub>O<sub>4</sub> to minimize reaction of the La and Fe with the support<sup>11, 21</sup>. Unfortunately, the crystallinity of the MgAl<sub>2</sub>O<sub>4</sub> interfered with the characterization of the films by XRD. To avoid this problem in the present study, we used a La-doped Al<sub>2</sub>O<sub>3</sub> support which has a relatively featureless XRD pattern, as shown in **Figure 1a**. This figure also shows XRD patterns for the Pt/LaFeO<sub>3</sub>/La-Al<sub>2</sub>O<sub>3</sub> sample after oxidation at 1073 K and after reduction at 1073 K. Both the oxidized and reduced samples show well-defined peaks associated with the LaFeO<sub>3</sub>, perovskite phase. Based on the linewidth of the peak at 33 degrees 2θ, the crystallite size of the perovskite phase was estimated to be between 9 and 11 nm. STEM/EDS images (**Figures S1 and S2**) show the La and Fe cover the support uniformly; and, since the average thickness of the LaFeO<sub>3</sub> film for this sample was only 0.5 nm, the perovskite crystals must be two-dimensional, as demonstrated previously for other ALD-deposited perovskite films<sup>13, 14</sup>. When compared with the JCPDS reference XRD pattern (no. 37-1493) for the LaFeO<sub>3</sub> phase, which is also included in **Figure 1**, the reflections for the perovskite film are shifted to slightly higher angles, ~0.8°, suggesting that there is a small contraction of the crystal lattice in the film that did not change with oxidation or reduction.

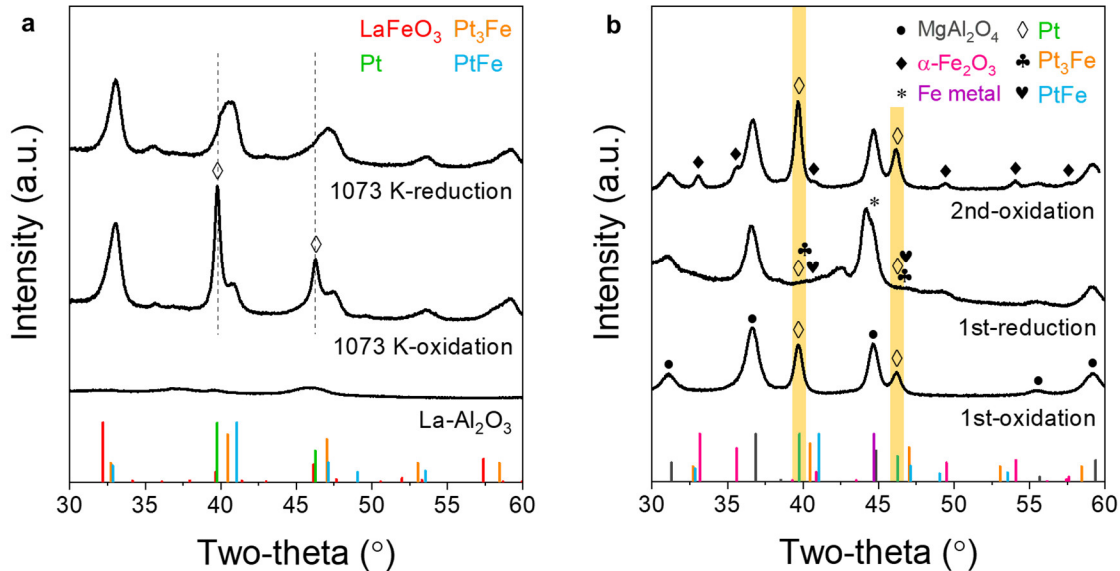


**Figure 1.** (a) XRD patterns of the oxidized and reduced Pt/LaFeO<sub>3</sub>/La-Al<sub>2</sub>O<sub>3</sub> after the first redox cycle. Reference patterns for LaFeO<sub>3</sub>, Pt, Pt<sub>3</sub>Fe, and PtFe are indicated at the bottom. The XRD pattern for La-doped Al<sub>2</sub>O<sub>3</sub> is shown together. (b) XRD patterns of Pt/FeO<sub>x</sub>/MgAl<sub>2</sub>O<sub>4</sub> after the first oxidation/reduction and the second oxidation. Reference patterns for MgAl<sub>2</sub>O<sub>4</sub>, α-Fe<sub>2</sub>O<sub>3</sub>, Pt, Pt<sub>3</sub>Fe, PtFe and Fe metal are shown at the bottom.

The major difference between the XRD patterns for the oxidized and reduced Pt/LaFeO<sub>3</sub>/La-Al<sub>2</sub>O<sub>3</sub> sample was in the features associated with Pt. Because the XRD pattern of the oxidized sample obtained after 5 redox cycles at 1073 K (See **Figure S3**) was identical to that after the first oxidation cycle, the changes that occurred upon oxidation or reduction appear to be reversible. The oxidized sample exhibited intense peaks at 39.7 and 46.2 degrees 2θ that are associated with metallic Pt; and, based on the peak width and the Scherrer equation, the average crystallite size of the Pt particles was 20 nm. In an apparent contradiction to this result, STEM/EDS images for the oxidized sample in **Figure S1** indicate that the Pt was well dispersed. A more detailed analysis of the TEM data is provided elsewhere<sup>11</sup>. Upon reduction at 1073 K, the metallic Pt peaks disappeared. An overlapping perovskite feature near 40 degrees 2θ makes definitive assignments difficult but the increased intensity in this region suggests that Pt has reacted with Fe in the perovskite film to form either Pt<sub>3</sub>Fe or PtFe intermetallic compounds, since these show peaks

in this same region. The XRD results shown here for Pt/LaFeO<sub>3</sub>/La-Al<sub>2</sub>O<sub>3</sub> are similar to what was reported previously for Pt/LaFeO<sub>3</sub>/MgAl<sub>2</sub>O<sub>4</sub><sup>11</sup>. That study observed narrow diffraction peaks for metallic Pt on the oxidized sample without large particles being observed by electron microscopy. Reversible disappearance of metallic Pt peaks was reported following high-temperature reduction, but an intense peak from the MgAl<sub>2</sub>O<sub>4</sub> prevented the observation of what are likely Pt-Fe intermetallic phases.

FT measurements were performed for a similar, Pt/LaFeO<sub>3</sub>/MgAl<sub>2</sub>O<sub>4</sub> sample to estimate the amount of Fe involved in the reduction process. After reduction at 1073 K for 1 h in a 10% H<sub>2</sub>-He mixture, the amount of O<sub>2</sub> required to re-oxidize LaFeO<sub>3</sub>/MgAl<sub>2</sub>O<sub>4</sub> was 90 μmol O<sub>2</sub>/g, while 385 μmol O<sub>2</sub>/g was required for re-oxidation of Pt/LaFeO<sub>3</sub>/MgAl<sub>2</sub>O<sub>4</sub> (**Table 2**). Since XRD showed that the Pt remained metallic after this oxidation treatment, the additional 295 μmol O<sub>2</sub>/g for the Pt-containing sample must be associated with reoxidation of the Fe in the LaFeO<sub>3</sub>. This amount of oxygen corresponds to 1.8 O/Pt. For reduction of Fe<sup>3+</sup> to metallic Fe, the value would be 1.5 O/Fe; therefore, reoxidation of reduced Pt/LaFeO<sub>3</sub>/MgAl<sub>2</sub>O<sub>4</sub> is consistent with forming a Pt-Fe intermetallic.

**Table 2.** Oxygen uptakes measured at 1073 K for the samples reduced at 1073 K.

Sample	Metal moles (± 10 μmol/g)	Oxygen taken up (±20 μmol oxygen/g)	Oxygen-to-metal ratio (excludes LaFeO <sub>3</sub> )
LaFeO <sub>3</sub> /MgAl <sub>2</sub> O <sub>4</sub>	-	90	-
Pt/LaFeO <sub>3</sub> /MgAl <sub>2</sub> O <sub>4</sub>	159	385	1.8:1

To gain additional insights into Pt-LaFeO<sub>3</sub> interactions, XRD patterns of an oxidized and reduced Pt/FeO<sub>x</sub>/MgAl<sub>2</sub>O<sub>4</sub> sample were also obtained and are displayed in **Figure 1b**. (The MgAl<sub>2</sub>O<sub>4</sub> support was used in this case to minimize the effects of FeO<sub>x</sub> reaction with Al<sub>2</sub>O<sub>3</sub><sup>24</sup>.) After the initial oxidation, only peaks associated with the MgAl<sub>2</sub>O<sub>4</sub> support and Pt (39.7 and 46.2 degrees 2θ) were observed. There were no observable peaks associated with a FeO<sub>x</sub> phase, likely because the 0.5-nm film was thinner than the coherence length of the X-rays. Reduction at 1073 K caused the Pt peaks to disappear, replaced by a feature at ~44.6 degrees 2θ that also overlaps

with a peak from the  $\text{MgAl}_2\text{O}_4$ . Because the Fe:Pt ratio was large, the position of the line associated with the metallic phase was essentially that of metallic Fe, shifted  $\sim 3.5$  degrees from peaks corresponding to  $\text{PtFe}$  and  $\text{Pt}_3\text{Fe}$ . It is noteworthy that the same conditions that effectively reduced the  $\text{FeO}_x$  film to metallic Fe did not significantly reduce the Fe in  $\text{LaFeO}_3$ . Even though the bulk Fe:Pt ratios were similar in the  $\text{Pt/LaFeO}_3/\text{La-Al}_2\text{O}_3$  and  $\text{Pt/FeO}_x/\text{MgAl}_2\text{O}_4$  samples, the metallic phase was Pt rich on the  $\text{Pt/LaFeO}_3/\text{La-Al}_2\text{O}_3$  sample and Fe rich on the  $\text{Pt/FeO}_x/\text{MgAl}_2\text{O}_4$  sample. After re-oxidation of the  $\text{Pt/FeO}_x/\text{MgAl}_2\text{O}_4$  sample at 1073 K, the Pt peaks were restored with increased intensity and a decreased width, implying growth in the average Pt particle size. Small peaks associated with  $\alpha\text{-Fe}_2\text{O}_3$  were also observed on the re-oxidized sample. The growth of large Pt particles and  $\text{Fe}_2\text{O}_3$  crystallites following redox cycling is consistent with STEM images for  $\text{Pt/FeO}_x/\text{MgAl}_2\text{O}_4$  that have been published previously<sup>11</sup>.

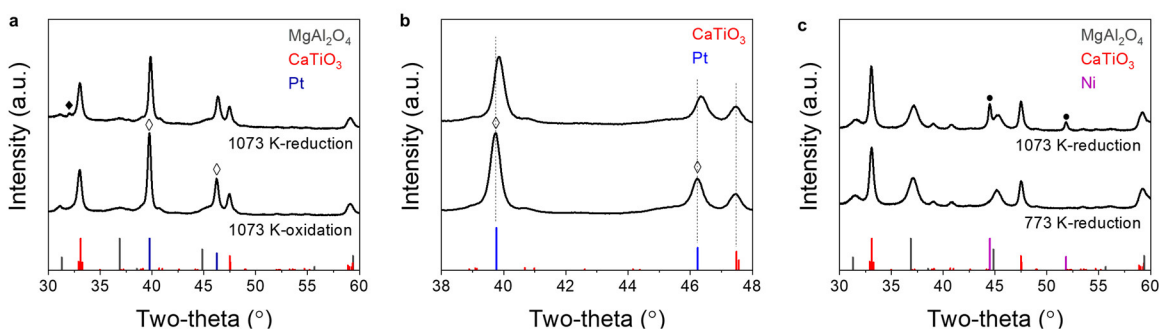


**Figure 2.** (a) XRD patterns of the oxidized and reduced  $\text{Pt/CaTiO}_3/\text{MgAl}_2\text{O}_4$  catalysts after the first redox cycle. Reference patterns for  $\text{MgAl}_2\text{O}_4$ ,  $\text{CaTiO}_3$  and Pt are indicated at the bottom. (b) XRD patterns with a magnified view of (a). Characteristic peaks for Pt and  $\text{Ca(OH)}_2$  are denoted by the empty diamond and solid diamond symbols, respectively. (c) XRD patterns of the  $\text{Ni/CaTiO}_3/\text{MgAl}_2\text{O}_4$ .  $\text{Ni/CaTiO}_3/\text{MgAl}_2\text{O}_4$  was subjected to the first redox cycle at 1073 K, after which it was reduced at 773 K or 1073 K. The reference XRD patterns for  $\text{MgAl}_2\text{O}_4$ ,  $\text{CaTiO}_3$  and Ni are indicated at the bottom. Characteristic peaks for Ni are marked by the solid circle symbols.

#### *Pt-CaTiO<sub>3</sub>, Ni-CaTiO<sub>3</sub>*

$\text{Pt/CaTiO}_3/\text{MgAl}_2\text{O}_4$ <sup>19</sup> and  $\text{Ni/CaTiO}_3/\text{MgAl}_2\text{O}_4$ <sup>18</sup> have been investigated in detail previously and were found to be similar to  $\text{Pt/LaFeO}_3/\text{MgAl}_2\text{O}_4$  in that catalysts oxidized at 1073 K were inactive for the reactions of interest while catalysts reduced at 1073 K were active. The  $\text{CaTiO}_3$ -containing catalysts also maintained their catalytic activity after 5 redox cycles at 1073 K.

To determine whether there might be similarities to their LaFeO<sub>3</sub> counterparts, we first re-examined these catalysts by XRD, with results shown in **Figure 2**. At first inspection, the diffraction patterns for oxidized and reduced Pt/CaTiO<sub>3</sub>/MgAl<sub>2</sub>O<sub>4</sub>, **Figure 2a**, are very similar. In addition to the peaks for MgAl<sub>2</sub>O<sub>4</sub>, both show features that can be assigned to Pt and CaTiO<sub>3</sub>. The reduced sample showed possible evidence for a small amount of Ca(OH)<sub>2</sub> at 32 degrees 2θ, but there were no other obvious differences in the pattern. However, closer examination of the peak positions for Pt, shown in **Figure 2b**, indicate that the position of Pt peak shifted to higher angles after reduction, while the CaTiO<sub>3</sub> peaks remained fixed. The Pt peak shift is consistent with partial alloying of Pt with Ti.

Additional evidence for reaction of Pt with Ti is provided by the STEM-EDS images of Pt/CaTiO<sub>3</sub>/MgAl<sub>2</sub>O<sub>4</sub> in **Figures 3 and 4**. The oxidized sample (**Figure 3**) shows two Pt particles that are between 20 and 40 nm in size. More important for this discussion, the EDS signals of the underlying Ca and Ti are relatively uniform and do not match up with the Pt particles. For the reduced sample (**Figure 4**), there is a clear correspondence between the EDS maps for Pt and Ti. While there appear to be areas of concentrated Ca also, possibly formed by decomposition of CaTiO<sub>3</sub>, the EDS signal for Ca does not match up with the Pt. These results suggest that interactions with Pt act as a driving force for partial decomposition of the perovskite in the vicinity of the Pt. The interactions also appear to change the shape of the Pt particles, from spherical to rhombohedral, as noted in the earlier study<sup>19</sup>. Since this sample in Figures 3 and 4 had been redox cycled 5 times, the differences between these two images are reversible, implying that any decomposition of the perovskite is reversible.

XRD of the oxidized and reduced Ni/CaTiO<sub>3</sub>/MgAl<sub>2</sub>O<sub>4</sub> sample, obtained after 5 redox cycles at 1073 K, are reported in **Figure 2c**. In addition to the features associated with MgAl<sub>2</sub>O<sub>4</sub> and CaTiO<sub>3</sub>, the reduced sample exhibits a peak for metallic Ni while the oxidized sample does not. STEM-EDS on identical samples were reported previously<sup>22</sup>; and, unlike the case for Pt/CaTiO<sub>3</sub>/MgAl<sub>2</sub>O<sub>4</sub>, there was no evidence of movement of the Ti towards the reduced Ni. This is further evidence that the apparent decomposition of the perovskite in Pt/CaTiO<sub>3</sub>/MgAl<sub>2</sub>O<sub>4</sub> is driven by interactions with the Pt.

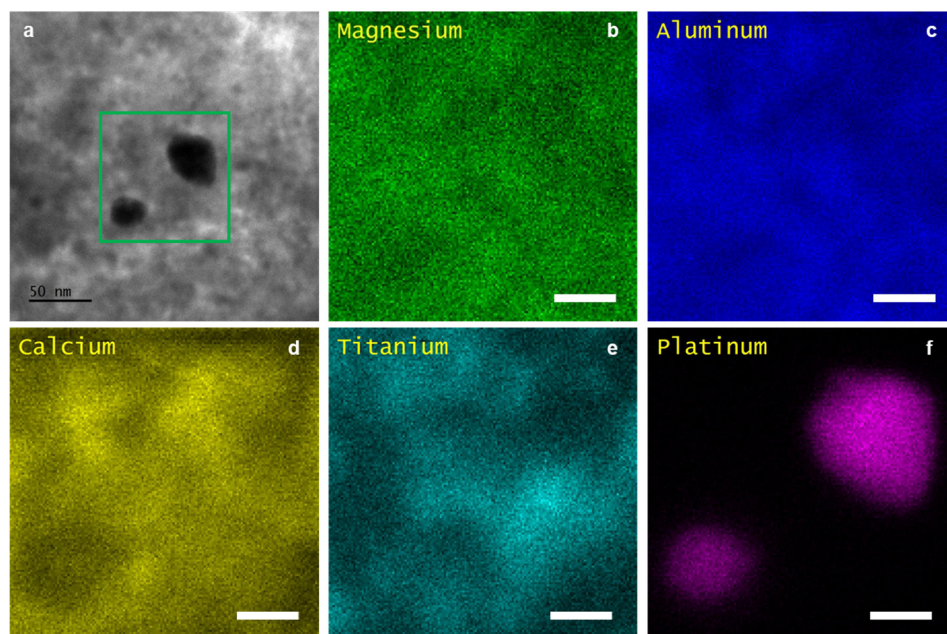


**Figure 3.** STEM and EDS image of Pt/CaTiO<sub>3</sub>/MgAl<sub>2</sub>O<sub>4</sub> after 5 redox cycles, finishing with an oxidation at 1073 K. The scale bar indicates 20 nm.

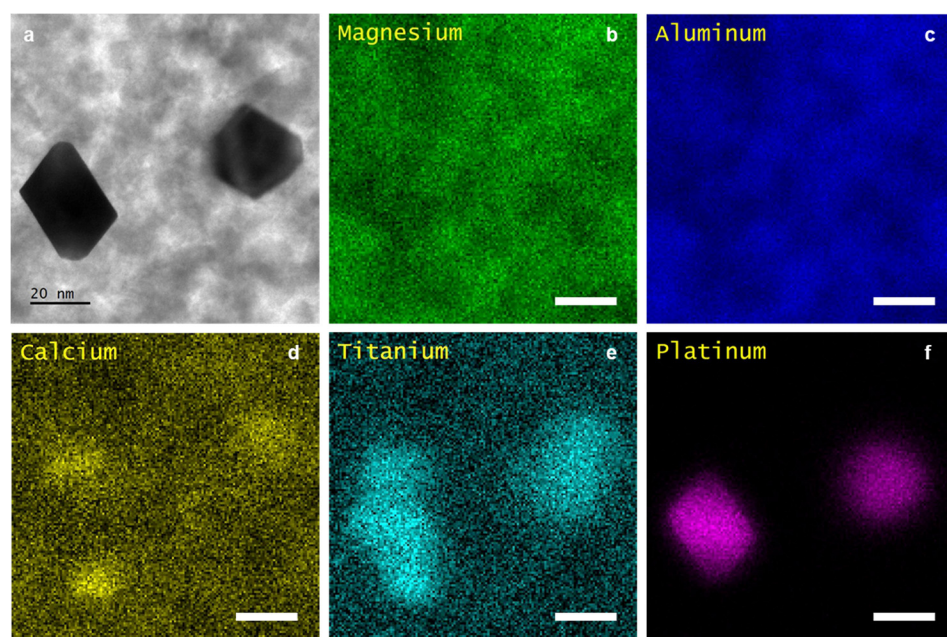


**Figure 4.** STEM and EDS image of Pt/CaTiO<sub>3</sub>/MgAl<sub>2</sub>O<sub>4</sub> after 5 redox cycles, finishing with reduction at 1073 K. The scale bar indicates 20 nm.

## ***Reactivity***

In past studies, perovskite-supported catalysts were observed to show higher rates than their conventional counterparts for some reactions but much lower rates for other reactions <sup>19</sup>. Rates on the perovskite-supported metals also depended dramatically on whether the catalyst had been oxidized or reduced at high temperatures prior to the rate measurements. Therefore, to gain insights into the catalytic properties of these materials, we measured differential rates for a number of reactions on both the reduced and oxidized catalysts.

### *Pt-LaFeO<sub>3</sub>*

To provide a baseline for the Pt/LaFeO<sub>3</sub>-based catalysts, rates were measured for the Pt/MgAl<sub>2</sub>O<sub>4</sub> catalysts listed in **Table 1**, as well as for Pt/FeO<sub>x</sub>/MgAl<sub>2</sub>O<sub>4</sub> and Pt/Bulk LaFeO<sub>3</sub>. The Pt/MgAl<sub>2</sub>O<sub>4</sub> catalysts differed in the calcination temperature used to pretreat them, which in turn affected the Pt dispersion. If support effects with LaFeO<sub>3</sub> are related to structure, rates should also change with particle size. Measurements on Pt/FeO<sub>x</sub>/MgAl<sub>2</sub>O<sub>4</sub> were used to determine the effect of alloying. To differentiate thin-film perovskites from bulk LaFeO<sub>3</sub>, measurements on Pt/Bulk LaFeO<sub>3</sub> allow one to distinguish differences between thin-film and bulk LaFeO<sub>3</sub>.

Differential rates for CO oxidation on Pt/LaFeO<sub>3</sub>/La-Al<sub>2</sub>O<sub>3</sub> are shown in **Figure 5a**. Rates were obtained after the initial oxidation at 1073 K and reduction at 1073 K and after 5 redox cycles. As reported previously, the LaFeO<sub>3</sub>-supported catalyst exhibited low activity after oxidation; but rates increased dramatically following reduction. While rates after 5 redox cycles decreased by roughly a factor of two on reduced Pt/LaFeO<sub>3</sub>/La-Al<sub>2</sub>O<sub>3</sub>, previous work showed that similar redox cycling of Pt/MgAl<sub>2</sub>O<sub>4</sub> catalysts decreased rates by approximately 100 <sup>11</sup>. Furthermore, specific rates based on catalyst mass were similar for the reduced Pt/LaFeO<sub>3</sub>/La-Al<sub>2</sub>O<sub>3</sub> and the fresh Pt/MgAl<sub>2</sub>O<sub>4</sub> (Rates for Pt/MgAl<sub>2</sub>O<sub>4</sub> are reported in **Figure S4**). Because the surface area of the Pt/Bulk LaFeO<sub>3</sub> catalyst was low, a direct comparison of rates for Pt/Bulk LaFeO<sub>3</sub> and Pt/LaFeO<sub>3</sub>/La-Al<sub>2</sub>O<sub>3</sub> was not possible; however, it is noteworthy that CO oxidation rates on a reduced Pt/Bulk LaFeO<sub>3</sub> catalyst were also dramatically higher than on its oxidized counterpart (**Figure S5**), showing that the bulk and thin-film catalysts show very similar characteristics.

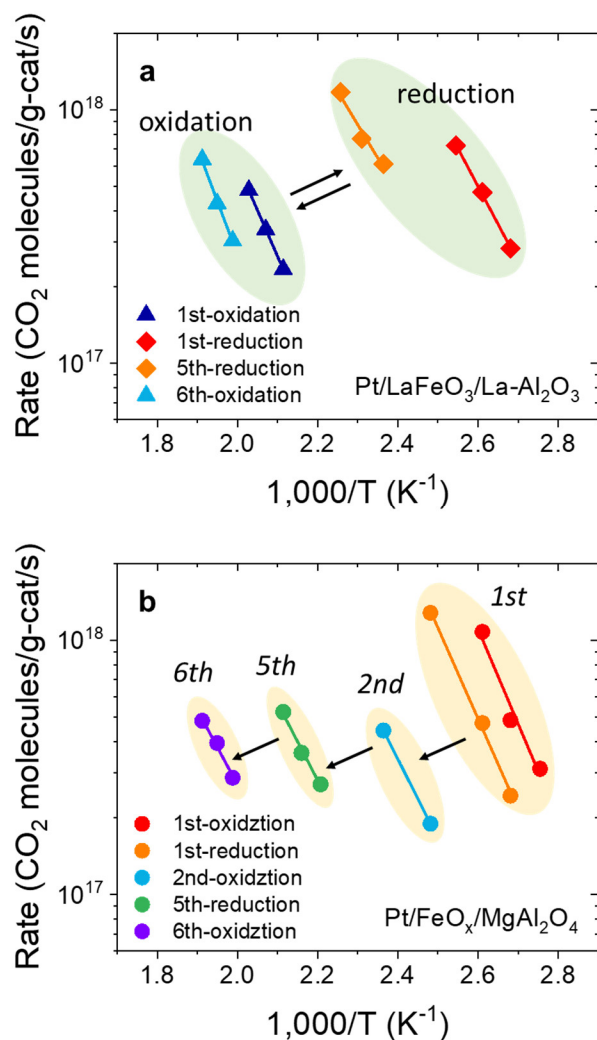


**Figure 5.** Differential rates for CO oxidation in 28 Torr CO and 14 Torr O<sub>2</sub> over (a) Pt/LaFeO<sub>3</sub>/La-Al<sub>2</sub>O<sub>3</sub> and (b) Pt/FeO<sub>x</sub>/MgAl<sub>2</sub>O<sub>4</sub>.

CO oxidation rates were also measured for the Pt/FeO<sub>x</sub>/MgAl<sub>2</sub>O<sub>4</sub> to determine the possible effect of Pt-Fe alloy formation, with an Arrhenius plot provided in **Figure 5b**. Unlike Pt/LaFeO<sub>3</sub>/La-Al<sub>2</sub>O<sub>3</sub>, the fresh Pt/FeO<sub>x</sub>/MgAl<sub>2</sub>O<sub>4</sub> sample showed high activity after oxidation at 1073 K. This agrees with literature observations that Fe<sub>2</sub>O<sub>3</sub> can promote CO oxidation over Pt<sup>25</sup> and also makes clear that the LaFeO<sub>3</sub> film has properties distinct from that of FeO<sub>x</sub>. High-temperature reduction, which should have formed a Pt-Fe alloy based on the earlier XRD results, did not significantly change the rates. Since the CO-oxidation atmosphere is oxidizing for Fe, it is

possible that the surface of the alloy is similar to that of the oxidized sample. However, the biggest difference between the FeO<sub>x</sub>- and LaFeO<sub>3</sub>-supported samples is that the Pt/FeO<sub>x</sub>/MgAl<sub>2</sub>O<sub>4</sub> sample was deactivated during redox cycling in a manner similar to that observed with Pt/MgAl<sub>2</sub>O<sub>4</sub>. Previously published STEM images showed that this deactivation is due to sintering of the Pt and Fe <sup>11</sup>.

As reported previously and shown in **Table 1**, CO adsorption was negligible on both the oxidized and reduced Pt/LaFeO<sub>3</sub>/La-Al<sub>2</sub>O<sub>3</sub>, even though CO oxidation rates were high. Because CO oxidation rates on conventional Pt are proportional to the Pt surface areas, Pt dispersions can be estimated by comparing the measured rates to specific rates reported in the literature <sup>26</sup>. As shown in **Table 1**, the agreement between dispersions measured by CO chemisorption and by comparison of specific rates is good for the Pt/MgAl<sub>2</sub>O<sub>4</sub> catalysts; however, the estimated dispersions were greater than 100% on the reduced Pt/LaFeO<sub>3</sub>/La-Al<sub>2</sub>O<sub>3</sub> and the fresh Pt/FeO<sub>x</sub>/MgAl<sub>2</sub>O<sub>4</sub> samples.

To understand how a catalyst that does not adsorb CO at room temperature could be active for CO oxidation, Pt/LaFeO<sub>3</sub>/MgAl<sub>2</sub>O<sub>4</sub> catalysts that had been oxidized or reduced at 1073 K were tested in *operando* CO oxidation DRIFTS experiments. **Figure 6a** shows the IR spectra of 1073-K, reduced Pt/LaFeO<sub>3</sub>/MgAl<sub>2</sub>O<sub>4</sub> under 50 Torr CO and 25 Torr O<sub>2</sub> at 298, 423, and 513 K. Notably, no CO adsorption was detected at 298 K, in agreement with CO chemisorption experiments. However, two sets of CO absorption bands at 2059–2065 cm<sup>-1</sup> and 2083–2090 cm<sup>-1</sup> appeared at higher temperatures, previously attributed to CO molecules linearly adsorbed in an a-top geometry on Pt<sup>0</sup> atoms on NPs surfaces <sup>27,28</sup>. This indicates that the surface of Pt NPs became exposed under reaction conditions in a temperature-activated process.

Exposure of the Pt sites was irreversible, as shown by the persistence of the adsorbed CO IR signals upon cooling the catalyst in the presence of inert gases to 298 K after CO oxidation. The signals shift to slightly higher wavenumbers at lower temperatures due to a stronger dipole-dipole coupling between adsorbed CO molecules <sup>27</sup>. Notably, the ratio of the observed CO IR bands is consistent with the presence of Pt nanoparticles smaller than 2 nm on average, predominantly exposing (111) facets, according to calculated CO IR spectra on a series of Pt nanoparticles of different sizes <sup>28</sup>. This is consistent with previous results on similar catalysts, where epitaxial growth of 1–2 nm Pt clusters was observed due to strong metal–support interaction

<sup>11</sup>.

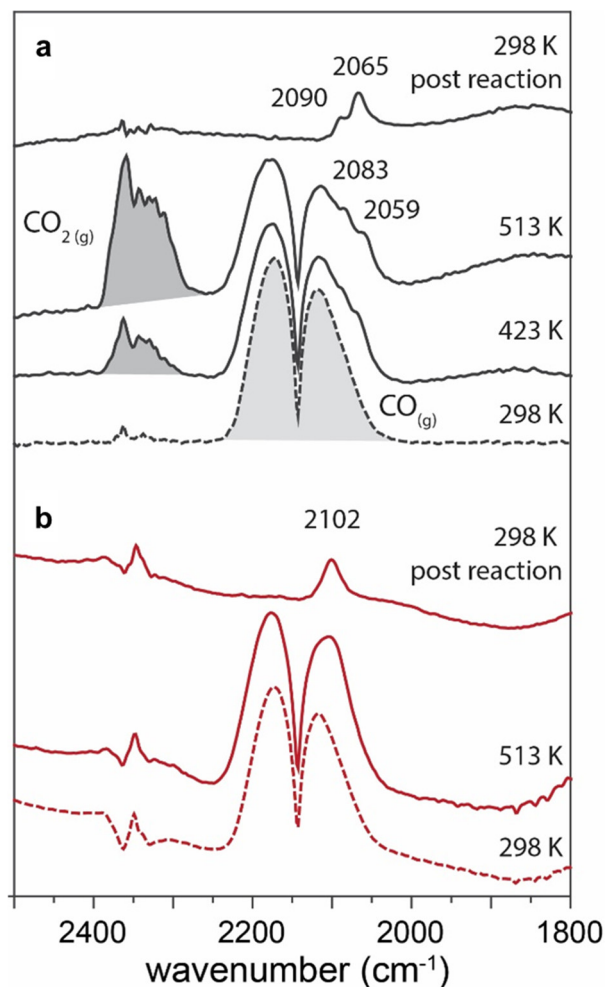


**Figure 6.** *Operando* diffuse reflectance infrared Fourier transform spectroscopy (DRIFTS) results during CO oxidation over Pt/LaFeO<sub>3</sub>/MgAl<sub>2</sub>O<sub>4</sub> after 1073 K (a) reduction and (b) oxidation. Conditions: 10 mg catalyst, 50 mL/min total flow, 50 Torr CO, 25 Torr O<sub>2</sub>, N<sub>2</sub> balance. CO<sub>2(g)</sub> signals in (b) are residuals from atmospheric background and are not correlated to the presence of CO<sub>(g)</sub>.

As shown by the absence of gaseous CO<sub>2</sub> IR signals, the 1073-K, oxidized Pt/LaFeO<sub>3</sub>/MgAl<sub>2</sub>O<sub>4</sub> catalyst showed negligible activity for CO oxidation at 513 K (**Figure 6b**). Similar to the pre-reduced sample, no CO adsorption was observed at 298 K. However, upon heating to 513 K, a single IR band centered at 2102  $\text{cm}^{-1}$  was observed, which can be assigned to CO linearly adsorbed on ionic Pt<sup>2+</sup><sup>29</sup>. Such adsorbed CO species persisted at RT, indicating an irreversible modification of the catalyst induced by exposure to CO oxidation conditions. Our IR results suggest that only Pt<sup>2+</sup> ions are exposed to the gas phase under CO oxidation conditions,

indicating the formation of a Pt-core@PtO-shell nanostructure. Overall, the results show that Pt<sup>0</sup> is more active than Pt<sup>2+</sup> in CO oxidation, and that both catalysts are irreversibly modified by CO at 513 K, leading to exposure of Pt. This indicates that, after reduction and oxidation, the PtO<sub>x</sub> NPs are covered by the support, possibly explaining the high thermal stability and sintering resistance.

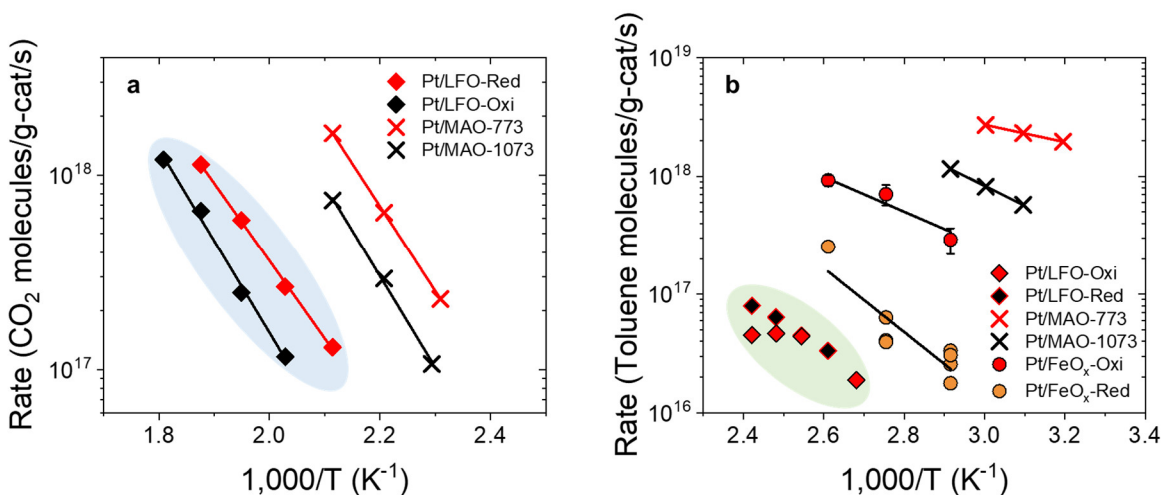


**Figure 7.** Differential rates for (a) propane oxidation and (b) toluene hydrogenation over Pt/LaFeO<sub>3</sub>/La-Al<sub>2</sub>O<sub>3</sub> (Pt/LFO), Pt/MgAl<sub>2</sub>O<sub>4</sub> (Pt/MAO), Pt/FeO<sub>x</sub>/MgAl<sub>2</sub>O<sub>4</sub> (Pt/FeO<sub>x</sub>). Samples designated Oxi and Red indicate that the final treatment involved either oxidation or reduction at 1073 K. The Pt/MAO data is for a sample that was oxidized at either 773 K or 1073 K.

While reduced, LaFeO<sub>3</sub>-supported Pt shows a high activity for CO oxidation, the details of the reaction mechanism must be quite different from that of ordinary supported Pt since CO adsorption is clearly different. To see how the presence of LaFeO<sub>3</sub> affects other reactions, we compared rates over Pt/LaFeO<sub>3</sub>/La-Al<sub>2</sub>O<sub>3</sub> and Pt/MgAl<sub>2</sub>O<sub>4</sub> for oxidation of propane and hydrogenation of toluene. Results for propane oxidation are shown in **Figure 7a**. First, propane oxidation appears to be somewhat structure sensitive, since rates on the Pt/MgAl<sub>2</sub>O<sub>4</sub> changed by only a factor of two when the catalyst was calcined to 1073 K, even though the dispersion changed by a factor of 15; however, structure does not appear to explain the very large differences between Pt/MgAl<sub>2</sub>O<sub>4</sub> and Pt/LaFeO<sub>3</sub>/La-Al<sub>2</sub>O<sub>3</sub>. Unlike the case for CO oxidation, rates on oxidized and reduced Pt/LaFeO<sub>3</sub>/La-Al<sub>2</sub>O<sub>3</sub> were nearly the same and roughly an order-of-magnitude lower than what was observed on Pt/MgAl<sub>2</sub>O<sub>4</sub>.

Rates for toluene hydrogenation over the Pt/LaFeO<sub>3</sub>/La-Al<sub>2</sub>O<sub>3</sub>, Pt/MgAl<sub>2</sub>O<sub>4</sub>, and Pt/FeO<sub>x</sub>/MgAl<sub>2</sub>O<sub>4</sub> catalysts are shown in **Figure 7b**. Again, the Pt/MgAl<sub>2</sub>O<sub>4</sub> catalysts were roughly 100 times more active than Pt/LaFeO<sub>3</sub>/La-Al<sub>2</sub>O<sub>3</sub>. Unlike the case for CO oxidation, high-temperature reduction and oxidation did not affect rates on Pt/LaFeO<sub>3</sub>/La-Al<sub>2</sub>O<sub>3</sub>. Results for Pt/FeO<sub>x</sub>/MgAl<sub>2</sub>O<sub>4</sub> help to explain why the reduced catalyst is not active. When Pt/FeO<sub>x</sub>/MgAl<sub>2</sub>O<sub>4</sub> was reduced at 1073 K to form the alloy, rates were nearly as low as that for Pt/LaFeO<sub>3</sub>/MgAl<sub>2</sub>O<sub>4</sub> catalysts; however, rates on the oxidized Pt/FeO<sub>x</sub>/MgAl<sub>2</sub>O<sub>4</sub> catalyst were more than a factor of 10 higher than those on Pt/LaFeO<sub>3</sub>/MgAl<sub>2</sub>O<sub>4</sub>.

The likely explanation for why oxidized Pt/LaFeO<sub>3</sub>/MgAl<sub>2</sub>O<sub>4</sub> is inactive for both propane oxidation and toluene hydrogenation is that the Pt is at least partially covered by or embedded within the LaFeO<sub>3</sub>. XRD showed that metallic Pt is clearly present when the sample was oxidized at 1073 K, and the low rates for toluene hydrogenation and propane oxidation are unlikely to be due to poor Pt dispersion.

#### *Pt-CaTiO<sub>3</sub>*

As discussed in the Introduction, metal-perovskite interactions are specific to the composition of the perovskite. With LaFeO<sub>3</sub>, the B-site cation can be reduced to its metallic form relatively easily. Since this is not true for CaTiO<sub>3</sub>, it was of interest to compare the catalytic properties of Pt/CaTiO<sub>3</sub> to Pt/LaFeO<sub>3</sub>. CO oxidation and 1-hexene hydrogenation were chosen as the test reactions for this study, with results shown in **Figure 8**.

CO oxidation rates on Pt/CaTiO<sub>3</sub>/MgAl<sub>2</sub>O<sub>4</sub> and Pt/LaFeO<sub>3</sub>/La-Al<sub>2</sub>O<sub>3</sub> showed similar characteristics, as demonstrated in **Figure 8a**. Both catalysts were activated by high-temperature reduction and deactivated by high-temperature oxidation. Rates on Pt/LaFeO<sub>3</sub>/La-Al<sub>2</sub>O<sub>3</sub> were significantly higher after reduction; and, since STEM measurements indicated that the Pt particle sizes were significantly smaller on Pt/LaFeO<sub>3</sub>/La-Al<sub>2</sub>O<sub>3</sub>, the difference between the two catalysts can be explained, at least in part, by particle size. Both showed high stability and maintained their activity after multiple redox cycles. 1-Hexene hydrogenation rates are shown for Pt/CaTiO<sub>3</sub>/MgAl<sub>2</sub>O<sub>4</sub>, Pt/MgAl<sub>2</sub>O<sub>4</sub>-1073 and Pt/LaFeO<sub>3</sub>/La-Al<sub>2</sub>O<sub>3</sub> in **Figure 8b**. Both perovskite-containing catalysts were dramatically less active than Pt/MgAl<sub>2</sub>O<sub>4</sub>-1073, independent of pretreatment. Since the Pt dispersion on Pt/MgAl<sub>2</sub>O<sub>4</sub>-1073 was already low, the low activity of the oxidized and reduced Pt/CaTiO<sub>3</sub>/MgAl<sub>2</sub>O<sub>4</sub> is not likely to be due simply to the dispersion.

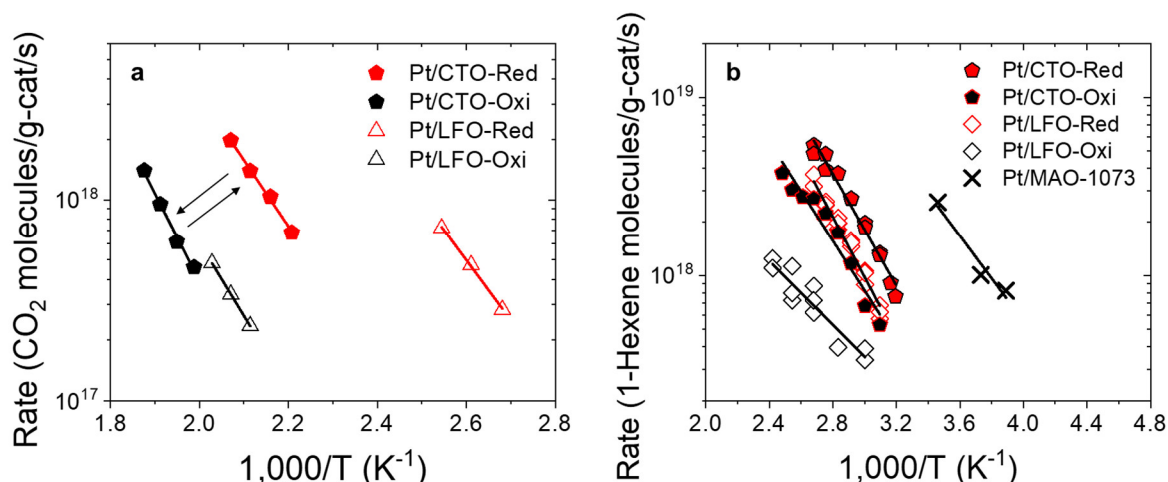


**Figure 8.** Differential rates for (a) CO oxidation and (b) 1-hexene hydrogenation over Pt/CaTiO<sub>3</sub>/MgAl<sub>2</sub>O<sub>4</sub> (Pt/CTO), Pt/LaFeO<sub>3</sub>/La-Al<sub>2</sub>O<sub>3</sub> (Pt/LFO), and Pt/MgAl<sub>2</sub>O<sub>4</sub> (Pt/MAO). Samples designated Oxi and Red indicate that the final treatment involved either oxidation or reduction at 1073 K. The Pt/MAO data is for a sample that was oxidized at either 773 K or 1073 K.

### *Ni-CaTiO<sub>3</sub>*

Because the metal-perovskite interactions are also specific to the metal, we also examined reactions on Ni/CaTiO<sub>3</sub>/MgAl<sub>2</sub>O<sub>4</sub> and compared the results to those of Ni/MgAl<sub>2</sub>O<sub>4</sub>. Since even conventional Ni catalysts must be reduced to be active, both catalysts were first oxidized at 1073 K, then reduced at temperatures between 773 K and 1073 K. Differential rates for MSR at 873 K are shown as a function of the reduction temperature on both catalysts in **Figure 9a**, and an Arrhenius plot of the rates on catalysts reduced at either high or low temperatures are reported in **Figure 9b**. The most obvious conclusion from these data is that higher reduction temperatures were required for the Ni/CaTiO<sub>3</sub>/MgAl<sub>2</sub>O<sub>4</sub> sample, consistent with an exsolution process. After reduction at 1073 K, Ni/MgAl<sub>2</sub>O<sub>4</sub> was somewhat more active but only by a factor of two.

Similar rate measurements were performed for 1-hexene hydrogenation, with results shown in **Figure 10**. Again, it was necessary to reduce the Ni/CaTiO<sub>3</sub>/MgAl<sub>2</sub>O<sub>4</sub> at higher temperatures; but the activities of the reduced Ni/CaTiO<sub>3</sub>/MgAl<sub>2</sub>O<sub>4</sub> and Ni/MgAl<sub>2</sub>O<sub>4</sub> were identical. This suggests that, unlike Pt/CaTiO<sub>3</sub>/MgAl<sub>2</sub>O<sub>4</sub>, the catalytic properties of the Ni are unaffected by the perovskite, except for increasing the temperatures required for reduction.

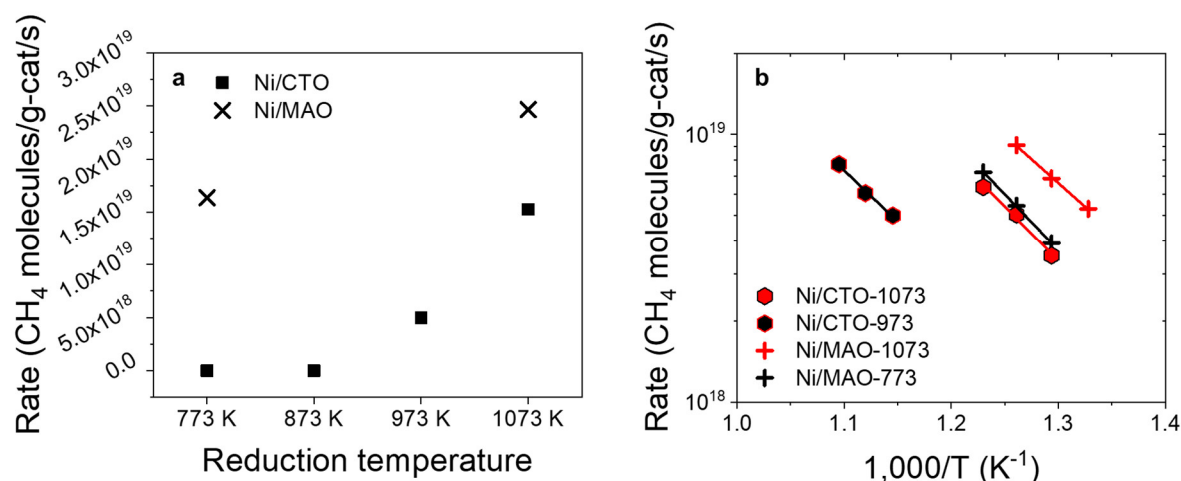


**Figure 9.** (a) Differential rates for the MSR reaction on Ni/MgAl<sub>2</sub>O<sub>4</sub> (Ni/MAO) and Ni/CaTiO<sub>3</sub>/MgAl<sub>2</sub>O<sub>4</sub> (Ni/CTO) catalysts at 873 K as a function of the reduction temperature. (b) Arrhenius plots for the MSR reaction on Ni/MgAl<sub>2</sub>O<sub>4</sub> and Ni/CaTiO<sub>3</sub>/MgAl<sub>2</sub>O<sub>4</sub> catalysts. Ni/CTO-1073 and Ni/CTO-973 experienced one redox cycle, followed by reduction at 1073 K or 973 K, respectively. Ni/MAO-1073 and Ni/MAO-773 experienced one redox cycle followed by reduction at 1073 K and 773 K, respectively.

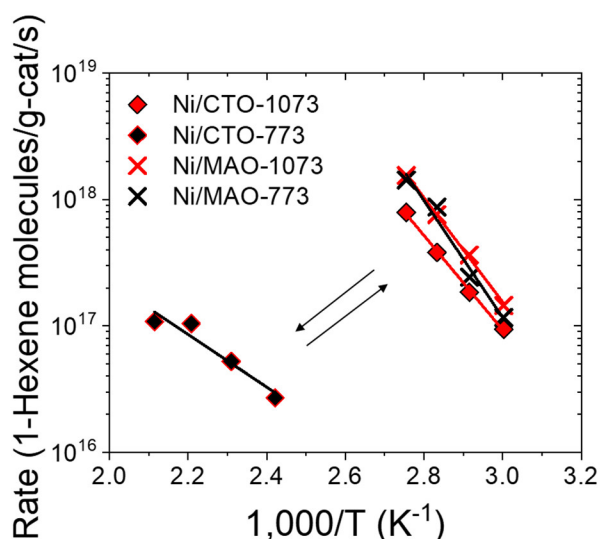


**Figure 10.** Differential rates for 1-hexene hydrogenation on Ni/MgAl<sub>2</sub>O<sub>4</sub> (Ni/MAO) and Ni/CaTiO<sub>3</sub>/MgAl<sub>2</sub>O<sub>4</sub> (Ni/CTO). Ni/CTO-1073 and Ni/CTO-773 indicate the samples experienced one redox cycle, followed by reduction at 1073 K or 773 K, respectively.

## Discussion

While it has been known for some time that interactions between a group 10 transition-metal catalyst and a perovskite oxide support, including exsolution phenomena in which the metal can ingress into the oxide under oxidizing conditions and egress under reducing conditions, can affect the structure and dispersion of the metal <sup>30</sup>, the results obtained here demonstrate that these interactions are quite complex and can impart unique catalytic properties beyond simply affecting the metal dispersion. Furthermore, these interactions are highly dependent on both the perovskite composition and the identity of the catalytic metal, making it difficult to generalize how the perovskite will affect activity for any particular reaction.

At least some of the novel properties for these systems appear to be due to the formation of intermetallic compounds, such as Pt-Fe; but the intermetallic compounds are not catalytically identical to conventional alloys. One likely reason for this is that the A-site cations (e.g. La<sup>3+</sup>) effectively lock the B-site element in place. For example, when Pt was deposited on FeO<sub>x</sub>, both Pt and Fe were able to sinter into larger particles; but this did not happen with the LaFeO<sub>3</sub> support. A second reason is that the Pt-Fe intermetallics formed on the LaFeO<sub>3</sub> appear to have a fixed stoichiometry. In addition to the XRD evidence suggesting the formation of Pt<sub>3</sub>Fe or PtFe compounds, the O<sub>2</sub> uptake measurements on the reduced catalyst showed 1.5 O/Pt, implying a reduction of one Fe<sup>3+</sup> for each Pt. Maintaining a fixed stoichiometry on alloy catalysts prepared by conventional means would be difficult.

Exactly how CaTiO<sub>3</sub> affects Pt is unclear. An earlier study had shown that the Pt particles were rhombohedral in shape when the catalyst was reduced at high temperatures <sup>19</sup>. In the present study, the lattice parameter of Pt was contracted, as shown by the shift in the XRD peak; and there was a segregation of Ti to the Pt as shown by the STEM measurements. The apparent decomposition of CaTiO<sub>3</sub> and migration of Ti to Pt indicates that strong bonding interactions between Pt and Ti must provide a driving force for Ti segregation; however, whether these data indicate actual Pt-Ti alloy formation or simply Pt in the presence of a reduced TiO<sub>x</sub> island is not clear. In either case, the catalytic properties of the Pt are modified. The Pt/CaTiO<sub>3</sub>/MgAl<sub>2</sub>O<sub>4</sub> catalyst that was active for CO oxidation showed dramatically lower rates for 1-hexene hydrogenation compared to a conventional Pt/MgAl<sub>2</sub>O<sub>4</sub>.

With Ni/CaTiO<sub>3</sub>/MgAl<sub>2</sub>O<sub>4</sub>, the catalyst properties more closely resemble those expected from the conventional view of exsolution. At least for the two reactions studied here, reduced Ni/CaTiO<sub>3</sub>/MgAl<sub>2</sub>O<sub>4</sub> showed similar rates to that of Ni/MgAl<sub>2</sub>O<sub>4</sub>. There was no evidence for decomposition of CaTiO<sub>3</sub> upon high-temperature reduction or Ti migration to Ni in STEM as there was with Pt. The coking tolerance observed in a previous study is likely due to the morphology of the of the Ni particles on CaTiO<sub>3</sub><sup>31</sup>.

The present study also provided additional evidence that thin-film perovskites interact with supported metals in a manner similar to that which occurs in bulk systems. In addition to the fact that catalysts oxidized at high temperatures were inactive and reduced materials were active for CO oxidation, reduced Pt catalysts on both bulk and thin-film LaFeO<sub>3</sub> were inactive for hydrogenation reactions. Because the perovskite films in this study were only 0.5 or 1.0 nm in thickness, corresponding to 1 or 2 unit cells, all atoms are effectively at the surface. The fact that high-temperature reduction is required to make these catalysts active suggests that the metal cations are incorporated into the perovskite lattice. High temperatures are required to remove the metal atoms from the lattice, not for the migration of the atoms from the bulk.

The use of perovskites as supports for transition-metal catalysts was initially viewed as simply a means to stabilize the dispersion of the metal. While the perovskite films certainly can play that role, the present work shows that perovskites also add additional complexity to these materials. To implement these materials, it is necessary to understand these metal-perovskite interactions, which will be specific to the particular metal and perovskite.

## Conclusions

The following conclusions can be drawn from our studies of CaTiO<sub>3</sub> and LaFeO<sub>3</sub> thin-film supports for Pt and Ni catalysts:

- 1) The perovskite thin films are able to stabilize Pt and Ni particle sizes during redox cycling at 1073 K.
- 2) The catalytic properties of Pt on bulk LaFeO<sub>3</sub> show similar characteristics to Pt on thin-film LaFeO<sub>3</sub>. In both cases, catalysts reduced at high temperatures show high activity for CO oxidation but are relatively inactive for hydrogenation reactions.
- 3) In some cases, high-temperature reduction can lead to local decomposition of the perovskite and formation of intermetallic compounds with supported Pt.

- 4) The nature of metal-perovskite interaction is metal and perovskite specific. Ni interacts with  $\text{CaTiO}_3$  differently from the way that Pt interacts with  $\text{CaTiO}_3$ ; Pt also interacts differently with  $\text{CaTiO}_3$  and  $\text{LaFeO}_3$ .

### Supporting Information

STEM/EDS images of Pt/LaFeO<sub>3</sub>/La-Al<sub>2</sub>O<sub>3</sub> after redox cycling; XRD patterns of Pt/LaFeO<sub>3</sub>/La-Al<sub>2</sub>O<sub>3</sub> after redox cycling; CO oxidation rates for Pt/LaFeO<sub>3</sub>/La-Al<sub>2</sub>O<sub>3</sub> and Pt/MgAl<sub>2</sub>O<sub>4</sub>; CO oxidation rates for Pt/bulk LaFeO<sub>3</sub> after redox cycling; Activation energy values for each of the reactions

### Acknowledgements

R.J.G. and J.M.V. are grateful to the Department of Energy, Office of Science, (Grant No. DE-SC0022238) for support of this work. S.L. thanks the Vagelos Institute for Energy Science and Technology (VIEST) for a Postdoctoral Fellowship. The authors acknowledge Chao Lin, Xinyu Mao, Ohhun Kwon, Woo-Jae Lee, and Reem Alqasayar at the University of Pennsylvania for assistance with sample preparation and characterization.

### References

- (1) Tanaka, H.; Tan, I.; Uenishi, M.; Kimura, M.; Dohmae, K. Regeneration of Palladium Subsequent to Solid Solution and Segregation in a Perovskite Catalyst: An Intelligent Catalyst. *Topics in Catalysis* **2001**, *16* (1), 63-70.
- (2) Nishihata, Y.; Mizuki, J.; Akao, T.; Tanaka, H.; Uenishi, M.; Kimura, M.; Okamoto, T.; Hamada, N. Self-regeneration of a Pd-perovskite catalyst for automotive emissions control. *Nature* **2002**, *418* (6894), 164-167.
- (3) Tanaka, H.; Taniguchi, M.; Kajita, N.; Uenishi, M.; Tan, I.; Sato, N.; Narita, K.; Kimura, M. Design of the intelligent catalyst for Japan ULEV standard. *Topics in Catalysis* **2004**, *30* (1), 389-396.
- (4) Uenishi, M.; Taniguchi, M.; Tanaka, H.; Kimura, M.; Nishihata, Y.; Mizuki, J.; Kobayashi, T. Redox behavior of palladium at start-up in the Perovskite-type LaFePdO<sub>x</sub> automotive catalysts showing a self-regenerative function. *Applied Catalysis B: Environmental* **2005**, *57* (4), 267-273.
- (5) Tanaka, H.; Taniguchi, M.; Uenishi, M.; Kajita, N.; Tan, I.; Nishihata, Y.; Mizuki, J. i.; Narita, K.; Kimura, M.; Kaneko, K. Self-Regenerating Rh- and Pt-Based Perovskite Catalysts for Automotive-Emissions Control. *Angewandte Chemie International Edition* **2006**, *45* (36), 5998-6002.
- (6) Jo, Y.-R.; Koo, B.; Seo, M.-J.; Kim, J. K.; Lee, S.; Kim, K.; Han, J. W.; Jung, W.; Kim, B.-J. Growth Kinetics of Individual Co Particles Ex-solved on SrTi<sub>0.75</sub>Co<sub>0.25</sub>O<sub>3-δ</sub> Polycrystalline Perovskite Thin Films. *Journal of the American Chemical Society* **2019**, *141* (16), 6690-6697.

- (7) Kim, K.; Koo, B.; Jo, Y.-R.; Lee, S.; Kim, J. K.; Kim, B.-J.; Jung, W.; Han, J. W. Control of transition metal–oxygen bond strength boosts the redox ex-solution in a perovskite oxide surface. *Energy & Environmental Science* **2020**, *13* (10), 3404-3411.
- (8) Malamis, S. A.; Harrington, R. J.; Katz, M. B.; Koerschner, D. S.; Zhang, S.; Cheng, Y.; Xu, L.; Jen, H.-W.; McCabe, R. W.; Graham, G. W.; et al. Comparison of precious metal doped and impregnated perovskite oxides for TWC application. *Catalysis Today* **2015**, *258*, 535-542.
- (9) Kim, K. J.; Han, H.; Defferriere, T.; Yoon, D.; Na, S.; Kim, S. J.; Dayaghi, A. M.; Son, J.; Oh, T.-S.; Jang, H. M.; et al. Facet-Dependent in Situ Growth of Nanoparticles in Epitaxial Thin Films: The Role of Interfacial Energy. *Journal of the American Chemical Society* **2019**, *141* (18), 7509-7517.
- (10) Lin, C.; Foucher, A. C.; Ji, Y.; Stach, E. A.; Gorte, R. J. Investigation of Rh–titanate (ATiO<sub>3</sub>) interactions on high-surface-area perovskite thin films prepared by atomic layer deposition. *Journal of Materials Chemistry A* **2020**, *8* (33), 16973-16984.
- (11) Mao, X.; Foucher, A. C.; Montini, T.; Stach, E. A.; Fornasiero, P.; Gorte, R. J. Epitaxial and Strong Support Interactions between Pt and LaFeO<sub>3</sub> Films Stabilize Pt Dispersion. *Journal of the American Chemical Society* **2020**, *142* (23), 10373-10382.
- (12) Mao, X.; Foucher, A. C.; Stach, E. A.; Gorte, R. J. “Intelligent” Pt Catalysts Based on Thin LaCoO<sub>3</sub> Films Prepared by Atomic Layer Deposition. *Inorganics* **2019**, *7* (9).
- (13) Kwon, O.; Foucher, A. C.; Huang, R.; Stach, E. A.; Vohs, J. M.; Gorte, R. J. Evidence for redispersion of Ni on LaMnO<sub>3</sub> films following high-temperature oxidation. *Journal of Catalysis* **2022**, *407*, 213-220.
- (14) Cao, T.; Kwon, O.; Lin, C.; Vohs, J. M.; Gorte, R. J. Two-Dimensional Perovskite Crystals Formed by Atomic Layer Deposition of CaTiO<sub>3</sub> on  $\gamma$ -Al<sub>2</sub>O<sub>3</sub>. *Nanomaterials* **2021**, *11* (9).
- (15) Onn, T. M.; Küngas, R.; Fornasiero, P.; Huang, K.; Gorte, R. J. Atomic Layer Deposition on Porous Materials: Problems with Conventional Approaches to Catalyst and Fuel Cell Electrode Preparation. *Inorganics* **2018**, *6* (1).
- (16) Mao, X.; Lin, C.; Graham, G. W.; Gorte, R. J. A Perspective on Thin-Film Perovskites as Supports for Metal Catalysts. *ACS Catalysis* **2020**, *10* (15), 8840-8849.
- (17) Neagu, D.; Oh, T.-S.; Miller, D. N.; Ménard, H.; Bukhari, S. M.; Gamble, S. R.; Gorte, R. J.; Vohs, J. M.; Irvine, J. T. S. Nano-socketed nickel particles with enhanced coking resistance grown in situ by redox exsolution. *Nature Communications* **2015**, *6* (1), 8120.
- (18) Lin, C.; Jang, J. B.; Zhang, L.; Stach, E. A.; Gorte, R. J. Improved Coking Resistance of “Intelligent” Ni Catalysts Prepared by Atomic Layer Deposition. *ACS Catalysis* **2018**, *8* (8), 7679-7687.
- (19) Lin, C.; Foucher, A. C.; Ji, Y.; Curran, C. D.; Stach, E. A.; McIntosh, S.; Gorte, R. J. “Intelligent” Pt Catalysts Studied on High-Surface-Area CaTiO<sub>3</sub> Films. *ACS Catalysis* **2019**, *9* (8), 7318-7327.
- (20) Oh, T.-S.; Rahani, E. K.; Neagu, D.; Irvine, J. T. S.; Shenoy, V. B.; Gorte, R. J.; Vohs, J. M. Evidence and Model for Strain-Driven Release of Metal Nanocatalysts from Perovskites during Exsolution. *The Journal of Physical Chemistry Letters* **2015**, *6* (24), 5106-5110.
- (21) Mao, X.; Foucher, A. C.; Stach, E. A.; Gorte, R. J. Changes in Ni-NiO equilibrium due to LaFeO<sub>3</sub> and the effect on dry reforming of CH<sub>4</sub>. *Journal of Catalysis* **2020**, *381*, 561-569.
- (22) Lin, C.; Foucher, A. C.; Stach, E. A.; Gorte, R. J. A Thermodynamic Investigation of Ni on Thin-Film Titanates (ATiO<sub>3</sub>). *Inorganics* **2020**, *8* (12).
- (23) Kwon, O.; Huang, R.; Cao, T.; Vohs, J. M.; Gorte, R. J. Dry reforming of methane over Ni supported on LaMnO<sub>3</sub> thin films. *Catalysis Today* **2021**, *382*, 142-147.

- (24) Shen, K.; Paige, J. M.; Kwon, O.; Gorte, R. J.; Vohs, J. M. Thermodynamic Properties of Iron Oxide Thin-Film Oxygen Carriers Prepared by Atomic Layer Deposition. *Industrial & Engineering Chemistry Research* **2021**, *60* (33), 12228-12234.
- (25) Liu, L.; Zhou, F.; Wang, L.; Qi, X.; Shi, F.; Deng, Y. Low-temperature CO oxidation over supported Pt, Pd catalysts: Particular role of FeO<sub>x</sub> support for oxygen supply during reactions. *Journal of Catalysis* **2010**, *274* (1), 1-10.
- (26) Rodriguez, J.; Wayne Goodman, D. High-pressure catalytic reactions over single-crystal metal surfaces. *Surface Science Reports* **1991**, *14* (1), 1-107.
- (27) Ding, K.; Gulec, A.; Johnson Alexis, M.; Schweitzer Neil, M.; Stucky Galen, D.; Marks Laurence, D.; Stair Peter, C. Identification of active sites in CO oxidation and water-gas shift over supported Pt catalysts. *Science* **2015**, *350* (6257), 189-192.
- (28) Lentz, C.; Jand, S. P.; Melke, J.; Roth, C.; Kaghazchi, P. DRIFTS study of CO adsorption on Pt nanoparticles supported by DFT calculations. *Journal of Molecular Catalysis A: Chemical* **2017**, *426*, 1-9.
- (29) Nie, L.; Mei, D.; Xiong, H.; Peng, B.; Ren, Z.; Hernandez Xavier Isidro, P.; DeLaRiva, A.; Wang, M.; Engelhard Mark, H.; Kovarik, L.; et al. Activation of surface lattice oxygen in single-atom Pt/CeO<sub>2</sub> for low-temperature CO oxidation. *Science* **2017**, *358* (6369), 1419-1423.
- (30) Cao, T.; Kwon, O.; Gorte, R. J.; Vohs, J. M. Metal Exsolution to Enhance the Catalytic Activity of Electrodes in Solid Oxide Fuel Cells. *Nanomaterials* **2020**, *10* (12).
- (31) da Fonseca, R. O.; Pongeggi, A. R.; Rabelo-Neto, R. C.; Simões, R. C. C.; Mattos, L. V.; Noronha, F. B. Controlling carbon formation over Ni/CeO<sub>2</sub> catalyst for dry reforming of CH<sub>4</sub> by tuning Ni crystallite size and oxygen vacancies of the support. *Journal of CO<sub>2</sub> Utilization* **2022**, *57*, 101880.